

Accepted Manuscript

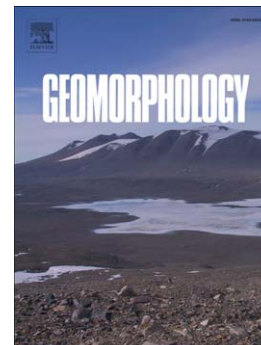
Nebkha flow dynamics and shadow dune formation

Patrick A. Hesp, Thomas A.G. Smyth

PII: S0169-555X(16)30213-6
DOI: doi:[10.1016/j.geomorph.2016.12.026](https://doi.org/10.1016/j.geomorph.2016.12.026)
Reference: GEOMOR 5872

To appear in: *Geomorphology*

Received date: 19 April 2016
Revised date: 24 October 2016
Accepted date: 27 December 2016



Please cite this article as: Hesp, Patrick A., Smyth, Thomas A.G., Nebkha flow dynamics and shadow dune formation, *Geomorphology* (2017), doi:[10.1016/j.geomorph.2016.12.026](https://doi.org/10.1016/j.geomorph.2016.12.026)

This is a PDF file of an unedited manuscript that has been accepted for publication. As a service to our customers we are providing this early version of the manuscript. The manuscript will undergo copyediting, typesetting, and review of the resulting proof before it is published in its final form. Please note that during the production process errors may be discovered which could affect the content, and all legal disclaimers that apply to the journal pertain.

© 2017. This manuscript version is made available under the CC-BY-NC-ND 4.0 license <http://creativecommons.org/licenses/by-nc-nd/4.0/>

Nebkha Flow Dynamics and Shadow Dune Formation**Patrick A. Hesp¹ and Thomas A.G. Smyth^{1,2}**

¹Beach and Dune Systems (BEADS) Laboratory,
School of the Environment, Flinders University,
Faculty of Science and Engineering,
Bedford Park, Adelaide, South Australia 5041.

Patrick.Hesp@flinders.edu.au

²Liverpool Hope University,
Hope Park, Liverpool L16 9JD,
United Kingdom.

Thomsmyth13@gmail.com

Abstract

In this study, wind flow is simulated via CFD over five ‘nebkha’ dune forms that range in shape from a cone, to a hemisphere (approximately) and to a dome in order to examine the structure of the wake zone formed downwind and the effect on the leeward flow separation zone and shadow dune formation. Dune height was fixed at 0.5 m while the nebkha diameter increased in 0.25 m increments from 0.5 m to 1.5 m and aspect ratio (h/D) from 1.0 to 0.3. The mean flow comprises an upwind region of reduced velocity which expands as nebkha width increases, high velocity marginal wings, and paired counter-rotating reversing vortices leeward of the nebkha. The point at which flow separation occurs moves further downwind as the nebkha diameter increases. The core regions of the reversing vortices are situated further downwind behind the smaller nebkha than in the case of the larger nebkha. These factors in combination allow for higher velocity perturbations (TKE) and narrower wake behind the smaller nebkha, and the suppression of downwind wake development in the case of the increasingly larger nebkha. Shadow dune length increases as nebkha width increases for lower incident velocity flow and is barely affected by nebkha width at higher flows. The extent of the leeward separation or wake zone, and hence shadow dune length, more strongly varies as a function of wind velocity.

Keywords: nebkha, shadow dunes, CFD flow modelling, shadow dune morphology

1.0 Introduction

Vegetation is critical to the development of many coastal, semi-arid and desert dunes such as nebkha, foredunes, blowouts and parabolic dunes and for the partial to complete stabilisation of dunefields (Nield and Baas, 2008; Mountney and Russell, 2009; Hesp et al., 2011; Hesp, 2013; Tsoar; 2013; Mayaud et al., 2016). Nebkha are a common dune type in almost all dunefields, arid to tropical humid, and coast to continental (Sokolov, 1884; Nichols, 1969; Hesp, 2004; Hesp and Walker, 2013; Ruz and Hesp, 2014). Nebkha are dunes formed by aeolian deposition within a discrete plant (Cooke et al., 1993), and they may reach 10 m in height in some deserts (Warren, 1988) but rarely above 3-4 m in coastal areas (M-H. Ruz, *pers. comm.*). The large, discrete, semi-vegetated to vegetated dune mounds observed in some coastal transgressive dunefields (e.g. Cooper, 1967; Hesp, 2013) may be mega-nebkha but they may also be vegetated remnant dunes and knobs (i.e. formed by aeolian erosion). Nebkha have also been termed nabkha, bush mounds, phytogenetic dunes and mounds (Cooke et al., 1993), foredune hillocks (Cooper, 1967), coppice and shrub-coppice dunes (Melton, 1940), (Cooke et al., 1993), hummocks (Sokolov, 1884), sand hummocks (Maun, 2009) and hedgehogs (Ranwell, 1972; Hesp and Smyth, in press). A shadow dune, which typically is characterised by a triangular- to teardrop-shaped ground plan and steep side slopes tapering downwind, may form downwind of the nebkha (Bagnold, 1954; Hesp, 1981) in both sand, sand and clay, and/or snow (Fig. 1). Shadow dunes have also been termed micro-dunes (Pidgeon, 1940), sand shadows or drifts (Bagnold, 1954; Nichols, 1969; Greeley and Iversen, 1985), tongue hills (Cooper, 1967), lee dunes (Cooke et al., 1993), and embryo dunes where they are forming in an incipient foredune zone (Salisbury, 1952; Hesp, 2002). Possibly some depositional streaks are also shadow dunes (cf. Thomas et al., 1981).

Nebkha and shadow dunes are important elements of the aeolian landscape because they can form in all sandy (and snow covered) lands. Their development has been associated with protection of oases and croplands (Zou et al., 2016), increasing aridity (e.g. Melton, 1940), desertification (Nickling and Wolfe, 1994; Wang et al., 2006), and human driven changes in rangelands (e.g. Rango et al., 2000). They form micro- to mesoscale habitats in some dune systems (e.g. El-Bana et al., 2002), and can be important for providing shelter, food and homes for a variety of fauna (Hesp and Mclachlan, 2000). Lines of nebkha form in some

coastal and desert regions and may in some cases lead to the formation of vegetated linear dunes (Tsoar, 2013). The initial vegetation colonisation and stabilisation of both coastal and desert dunefields may begin with nebkha formation (Hesp, 2013; Fig. 1). In relatively unidirectional to low directional variability wind regimes and locations (e.g. mountain gaps) shadow dunes may extend downwind over time and be quite stable and large features (Greeley and Iversen, 1985; Xiao et al., 2015). They have also been termed, or may evolve downwind into lee dunes, linear dunes and longitudinal dunes (Greeley and Iversen, 1985; Rubin and Hesp, 2009).

2.0 Flow around discrete roughness elements

As Gillies et al. (2014) note, the flow around cylinders and hemispheres (Sutton and McKenna-Neuman, 2008) has similarities to flow around nebkha, with one principal difference that nebkha are porous to various degrees (Dong et al., 2008; Mayaud et al., 2016). There are multiple studies of flow around discrete cylinders, pipes, flat plates and other obstacles or roughness elements both solid and porous (e.g. Kiya and Sasaki, 1983). Some of the relatively recent (~last 3 decades) work is reviewed in Niemann and Holscher (1990), Zdravkovich (1990), Vogel (1994), Williamson (1996), Sutton and McKenna-Neuman (2008), Bauer et al. (2013), Gillies et al. (2014), Stringer et al. (2014) McKenna-Neuman and Bédard (2015), and Chawdhury and Morgenthal, (2016).

The flow around a discrete cylinder and hemisphere tends to be characterised by six flow regions, namely: (i) an upwind region of stagnation pressure and reversing flow at and near the bed, (ii) an upwind region of accelerated flow over the top, (iii) a region of flow deflection or diversion and acceleration around the object and the possible development of a horseshoe vortex extending downwind around the margins of the cylinder forming the outer boundary of the wake zone, (iv) a separation or wake zone (or envelope) formed on the sides of the cylinder (location dependent on Reynolds number [Re]) and extending downwind behind the cylinder. Within the wake zone or separation envelope, (v) an arch vortex may form behind the cylinder and paired, opposed vortices form at the base, and (vi) trailing vortex pairs form downwind (Savory and Toy, 1986; Acarlar and Smith, 1987; Rodi, 1997; Meneghini et al., 2001; Xu et al., 2007; Sutton and McKenna-Neuman, 2008; Kharoua and Khezzar, 2013; McKenna-Neuman and Bédard, 2015; Tavakol et al., 2015). As noted by Vogel (1994, p. 93), above a Re of ~40 the vortices formed behind a cylinder alternately detach, “producing a wake of vortices with each rotating in a direction opposite that of its

predecessor farther downstream” creating a Von Kármán trail or vortex street (see e.g. Fig 4 in Catalano et al., 2003). This periodic shedding of vortices continues up to a Re of $\sim 100,000$ – $200,000$. Above a Re of $\sim 200,000$ to $250,000$ the wake narrows and becomes fully turbulent. The Von Kármán vortex pattern is antisymmetric when the aspect ratio of the cylinder (h/D where h is roughness element height and D is element diameter) is large, and becomes symmetric as the aspect ratio decreases (Sumner et al., 2004; McKenna-Neuman and Bédard, 2015). On average, the *mean flow* behind a cylinder, hemispheres and many other objects at relatively high Reynolds numbers (e.g. cubes; Luo et al., 2012, 2014; Bauer et al., 2013; Fu et al., 2015) comprises a pair of counter-rotating vortices at or near the bed (Tavakol et al., 2010, 2015).

The flow into, over and around a discrete plant (required to form a nebkha) is similar to that described above except that there can be considerable bleed flow through parts or all of the plant prior to sand deposition within the plant depending on plant morphology and density (Dong et al., 2008; Bauer et al., 2013; Mayaud et al., 2016; Hesp and Smyth, in press). Dong et al. (2008) show that the positions of the reverse vortices move in response to changes in shrub density with the reversing vortices situated further downwind at lower densities because the bleed flow pushes the reverse cells downwind. However, this depends entirely on how dense the lowermost portions of the plant near the bed are as illustrated by Mayaud et al. (2016). In natural plants exhibiting high density near the bed, little bleed flow will occur (Hesp, 1981), but with increasing height above the bed, the plant porosity and hence the degree of bleed flow typically increases. Below a critical plant density, bleed flow can dominate (Dong et al., 2008). The flow structure will also vary depending on the degree of cover and position of the vegetation on a nebkha, such that, for example, scour around the frontal base and sides is more likely where the plant cover does not reach or cover the basal circumference of the nebkha (Sutton and McKenna-Neuman, 2008; Hesp and Walker, 2013; McKenna-Neuman and Bédard, 2015).

Multiple studies of the wind flow, and particularly the shear stress partitioning and distribution, and drag around terrestrial plants have been conducted (e.g. Wolfe and Nickling, 1996; Wyatt and Nickling, 1997; Gillies et al., 2000, 2002, 2014; Li et al., 2008a, 2008b; Leenders et al., 2011; Yager and Schmeeckle, 2013), and many studies of flow in plants in aquatic environments have been carried out (e.g. Poggi et al., 2004, 2009; Bouma et al., 2007; Nepf, 2012 review; Ortiz et al., 2013; Okamoto et al., 2014; Chang et al., 2014; de Lima et

al., 2015). However, while there are many studies of the wake zone and associated flow structure around and downwind of obstacles, roughness elements, and discrete plants and vegetation patches (as above), very few studies have examined the dynamics of shadow dune formation behind a plant or nebkha (real or simulated). Additionally, flow around a blunt or curved solid object tends to produce marginal and downwind bed erosion (Sutton and McKenna-Neuman, 2008) while porous objects and plants tend to produce leeward deposition (Bauer et al., 2013). Hesp (1981) conducted a field and wind tunnel study of the mean flow around natural erect plants varying from 7 to 19 cm diameter and across a range of wind velocities from 5 – 20 m s⁻¹. He showed that a wake formed behind the plant and comprised symmetrically opposed reversing vortices within which a triangular shadow dune formed. Shadow dune height was dependent on plant basal (spanwise) width and sand repose angle as follows:

$$h = w/2 \tan \theta \quad (\text{eqn. 1})$$

where h is shadow dune height, w is plant width and $\tan \theta$ is the dune slope which obviously cannot be greater than $\sim 32^\circ$ for medium dry sand. Dune height is greatest at the immediate rear of the plant and tapers downwind as the shadow zone decreases in spanwise width (Fig 1C). Shadow dune length was a function of wind speed and plant width, but the relationship was not linear. Savory and Toy (1986) stated that the point downwind at which the wake terminates - the reattachment length or distance - was 1.1 times the dome diameter. However, this point increases with the aspect ratio h/D (Iversen et al., 1990; Palau-Salvador et al., 2009; McKenna-Neuman and Bédard, 2015), and depends on the surface roughness with the distance increasing as roughness increases (Kharoua and Khezzer, 2013). Gillies et al. (2014) demonstrated this where they showed that the presence of a porous vegetation cover on a nebkha reduced the rate at which the wind speed recovered to the freestream speed compared to the same nebkha mound once it was de-vegetated.

Luo et al. (2012) examined shadow dune formation behind cuboids, but to the authors' knowledge there has not been a study which examines the relationship between nebkha dimensions and shadow dune formation *per se*. Luo et al. (2012) state that shadow dunes are the least well understood of anchored dunes. In addition, the Hesp (1981) study was conducted with relatively low technology equipment compared to current technology, and exactly defining the wake flow structure and shadow dune length was difficult.

The aims of this study are to: (i) examine further the flow around various single or discrete dome shapes simulating nebkha via computational fluid dynamics (CFD) modelling, and (ii) examine the structure of the flow separation envelope or wake zone formed downwind of the nebkha wherein a shadow dune would form.

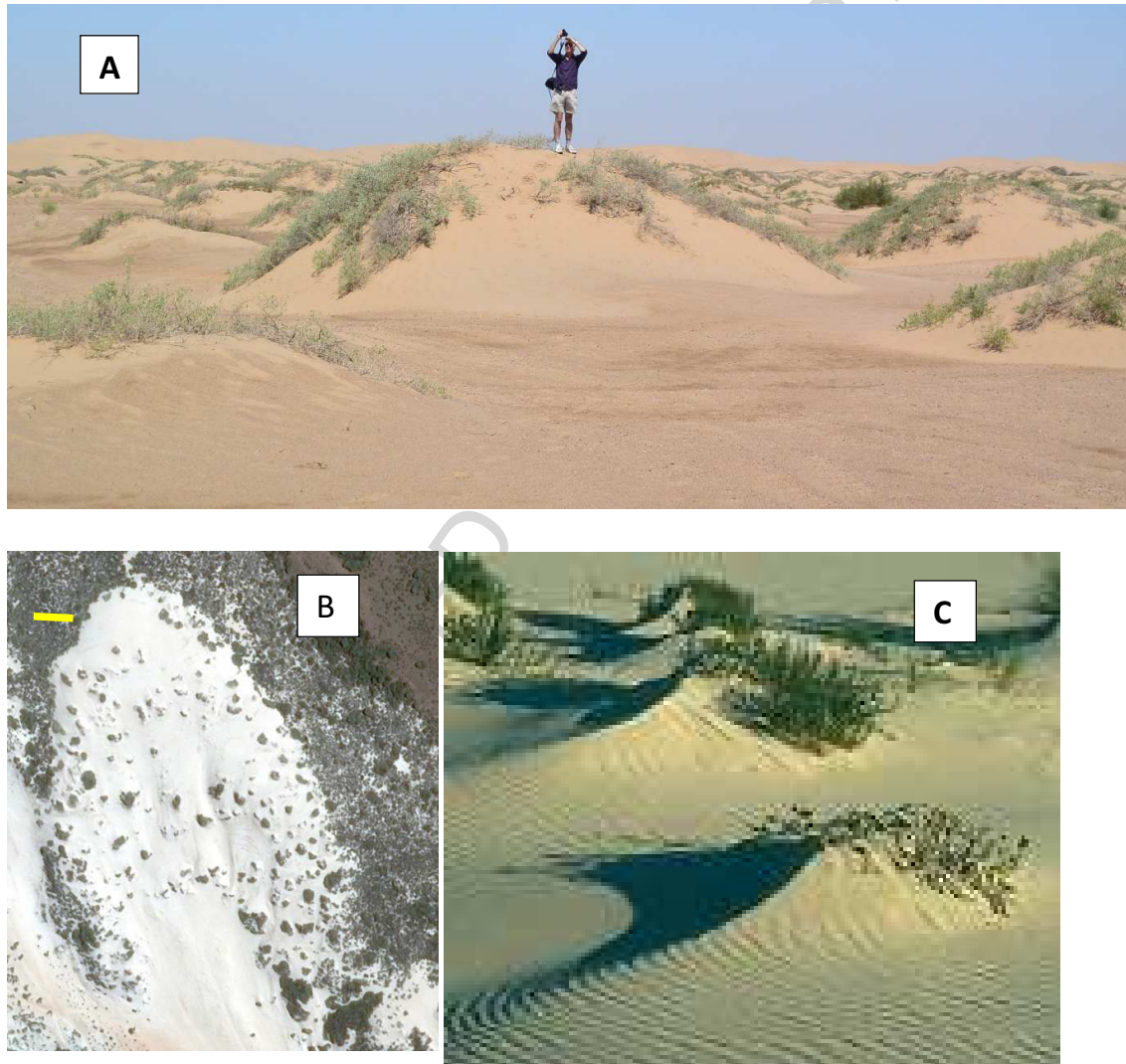


Figure 1: Various nebkha and shadow dunes. (A) Hemispheric nebkha in NW China (person is 1.8m tall). (B) Shadow dunes formed on a stabilising parabolic dune near Horrocks, Western Australia (28deg S; scale bar is 30m). (C) Shadow dunes formed downwind of small nebkha.

3.0 Methods

3.1 Nebkha Topography

Nebkha morphology can be highly variable in the field depending, among other things, on vegetation cover, and plant species form. However, the dune formed within a plant often roughly approximate cones, hemispheres and/or domes (Li et al., 2008a, b; Al-Awadhi and Al-Dousari, 2013; Gillies et al., 2014) as indicated in Fig. 1A. In this study, wind flow was simulated over five ‘nebkha’ dune forms that range in shape from a cone to a hemisphere (approximately) to a dome. This was considered reasonable since many nebkha approximate one of these shapes (see Fig. 1A). In order to keep one dimension constant and minimise computational time and complexity, the height of the dune was fixed at 0.5 m. The diameter of the nebkha increased in 0.25 m increments from 0.5 m to 1.5 m (Fig. 2).

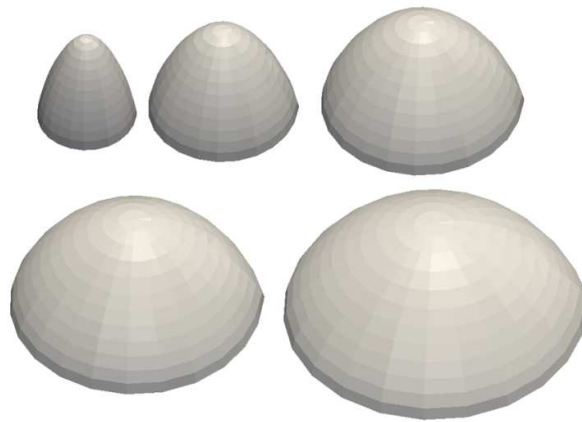


Figure 2. Simulated nebkha topographies over which wind flow was modelled. All dunes measured 0.5 m high and the diameter increased in increments of 0.25 m. The smallest nebkha cone is 0.5 m diameter. Aspect ratios (height/Diameter) range from 1.0, 0.66, 0.5, 0.4 and 0.33.

A mesh of each dune was created using the mesh generation utility, *snappyHexMesh*, included in the open source computational fluid dynamics (CFD) toolbox, OpenFOAM (Weller et al. 1998). Each mesh contained approximately 2.2 million cells and was meshed with increasing spatial resolution toward the dune shape, to a maximum of 0.00625 m (Fig. 3). The boundaries of the computational domain were spaced 5 m (10H) upwind, 25 m (50H) downwind, 12.5 m (25H) from the centre of the nebkha and 10 m (20H) high, containing 50 vertical levels, to ensure secondary wind flow patterns could be adequately resolved.

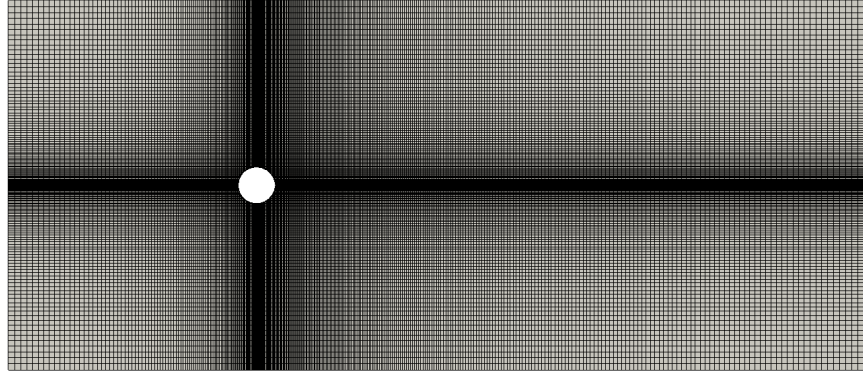


Figure 3. Mesh at the surface of the computational domain. Cell size decreased to a minimum size of 0.00625 m at the dune. The inlet boundary (left) is located 10H upwind of the dune while the downwind boundary is 50H downwind.

3.2 CFD methodology

All CFD modelling was performed using OpenFOAM (Weller et al. 1998). The SIMPLE (Semi-Implicit Method for Pressure Linked Equations) algorithm was used to solve the Navier-Stokes equations (Patankar and Spalding, 1972). This method produces a steady-state, averaged solution of flow. Turbulence was modelled using the Renormalization Group Theory (RNG) k - ϵ method which accounts for the smaller scales of motion and offers improved predictions for separated flows than the original k - ϵ model (ANSYS, 2013, Smyth, 2016). An upwind spatial discretisation scheme was employed to ensure all simulations achieved convergence. Calculations were considered complete once the residual of each iteration was lower than 0.0001 for U_x , U_y and U_z and wind speed in the lee of the dune varied by less than 0.01%.

3.2.1 Boundary conditions

In each simulation vertical profiles of wind speed (U), turbulent kinetic energy (k) and energy dissipation (ϵ) at the inlet boundary were defined assuming a constant shear velocity (u_*) value with height using equations 2, 3 and 4 (Richards and Hoxey, 1993; Blocken et al., 2007):

$$U(z) = \frac{u_*}{\kappa} \ln \left(\frac{z+z_0}{z_0} \right) \quad (\text{eqn. 2})$$

$$k(z) = \frac{u_*^2}{\sqrt{C_\mu}} \quad (\text{eqn. 3})$$

$$\varepsilon(z) = \frac{u_*^3}{\kappa(z+z_0)} \quad (\text{eqn. 4})$$

where z is the height above the surface, κ is the von Karman constant (0.42) (Richards and Hoxey, 1993; Blocken et al. 2007), z_0 is the surface roughness length and C_μ a constant of 0.09 (Richards and Hoxey, 1993; Jackson et al. 2011)

To examine how flow dynamics changed with wind speed, simulations were conducted using 5 values of u_* ranging from a minimum of 0.41 m s^{-1} to 1.11 m s^{-1} (Table 1), and a range of Reynolds numbers (Table 2). While 20 m s^{-1} ($u_* = 1.11 \text{ m s}^{-1}$) winds at 1 m above the surface are rare, they are not unknown in desert and coastal environments. For example, Hesp et al. (2013) measured wind speeds of 18 m s^{-1} at 1 m height on a foredune crest, and Smyth et al. (2013) measured 1-minute averages in excess of 20.8 m s^{-1} on a foredune slope in Western Ireland. For each simulation a surface surrounding the dune was prescribed a surface roughness constant (z_0) of 0.0005 m , the equivalent of a sand surface (Bagnold, 1954). The dune structure could only be assigned a maximum roughness length of 0.003125 m , as surface roughness length cannot exceed half the height of the smallest cell (cf. Blocken et al., 2007; Smyth, *in press*) (Fig. 3).

Shear Velocity (m s^{-1})	Wind Speed 1 m above surface (m s^{-1})
0.41	7.5
0.55	10
0.83	15
1.11	20

Table 1. Shear velocities (m s^{-1}) and equivalent wind speeds (m s^{-1}) at 1 m above the surface at the inlet of the computational domain for each simulation.

		Velocity (m s^{-1})			
		7.5	10	15	20
diameter r (m)	0.50	268,750	358,333	537,500	716,667
	0.75	403,125	537,500	806,250	1,075,000

1.00	537,500	716,667	1,075,000	1,433,333
1.25	671,875	895,833	1,343,750	1,791,667
1.50	806,250	1,075,000	1,612,500	2,150,000

Table 2. Resulting Reynolds numbers according to the range of velocities modelled (7.5 to 20 m s⁻¹) and the nebkha diameters(0.5 to 1.5m). The latter are all classified as fully turbulent. Reynolds number was defined as $Re = \frac{\rho v D}{\eta}$ where ρ is air density (1.29 kg m³), v is incident wind speed 1 m above the surface, D is diameter of the nebkha and η is air viscosity (0.000018 Pa.S).

3.3 Determination of the Shadow Dune Length

Hesp (1981) determined the length of the separation zone or wake region (within which the shadow dune would form) by measuring the point downwind on the centreline axis behind a plant where the velocity reached 4 m s⁻¹ at ~ 2 cm above the surface following Bagnold's (1954, p. 69) threshold velocity (cf. Hsu, 1973). This value was assumed to be the threshold wind speed at which sediment transport would again take place in the lee of the plant and shadow dune formation would cease. While Luo et al. (2012), for example, determined this position by estimating the point where the reversing cell streamlines converged, in this study the Hesp (1981) method was followed as it was considered to be more accurate than estimating a streamline convergence point, and to allow comparison between those results and the CFD simulations conducted herein.

3.4 Limitations of the Modelling

This study includes some key constraints and assumptions that should be considered when examining the results. First, the rule regarding sand deposition to the lee of the nebkha or 'dune': the shadow dune is assumed to terminate downwind when the flow velocity reaches 4 m s⁻¹ at 0.1 m above the bed. In reality in the field this termination point also depends on grain size and at what height the measurement is made. Second, in the field, as a shadow dune begins to form in the triangular wake (separation) zone behind the nebkha, there is a positive feedback between form and flow such that the symmetrical paired vortices are increasingly forced to flow upslope as the shadow dune develops. The vortical structures

therefore likely change somewhat as shadow dune formation occurs. In this modelling study we assume the shadow dune will grow within the original wake or separation zone, and that the shape or size of this zone does not change. Third, the surface of the modelled nebkha dune is relatively smooth. It has no vegetation present and therefore bleed flow typical of flow through a plant on a nebkha does not occur. The absence of vegetation also means that it cannot trap sand and grow upward over time, along with the formation of the shadow dune. This is not a critical issue since at any one day in the field, a nebkha and its attendant vegetation will induce a shadow dune related to its size and shape and porosity on that day. Given these constraints and assumptions, in essence, the results developed here are a first approximation only.

4.0 Nebkha Flow Dynamics

The instantaneous flow behind a nebkha as simulated here is characterised by turbulent vortices. However, the mean flow is typically characterised by two symmetrically opposed vortices within the flow separation wake zone at these high Reynolds numbers (Fig. 4a). Fig. 4b provides a snapshot of the turbulent character of the wake behind a 1 m-diameter nebkha for comparison. Only the mean flow conditions are referred to in the following study.

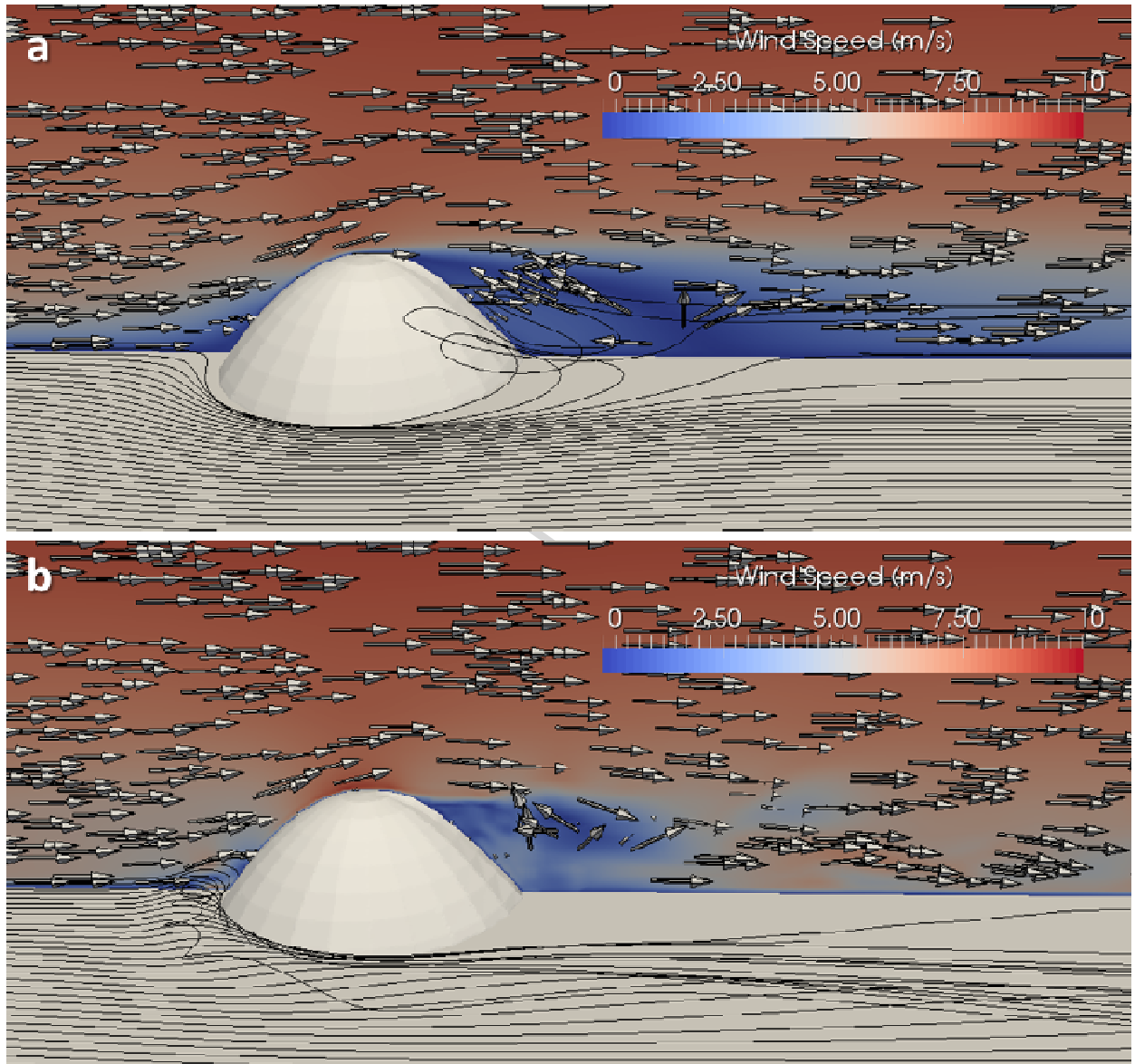


Figure 4: Average (a) and instantaneous (b) plots of wind flow velocity around a 1 m-high nebkha dome, calculated using a Reynolds-Averaged Navier-Stokes (RANS) and Large Eddy Simulation (LES). Plot (b) demonstrates the formation of turbulent eddies and flow structures in lee of the form which are not present in simulations conducted for this study as a RANS (plot a) model has been employed.

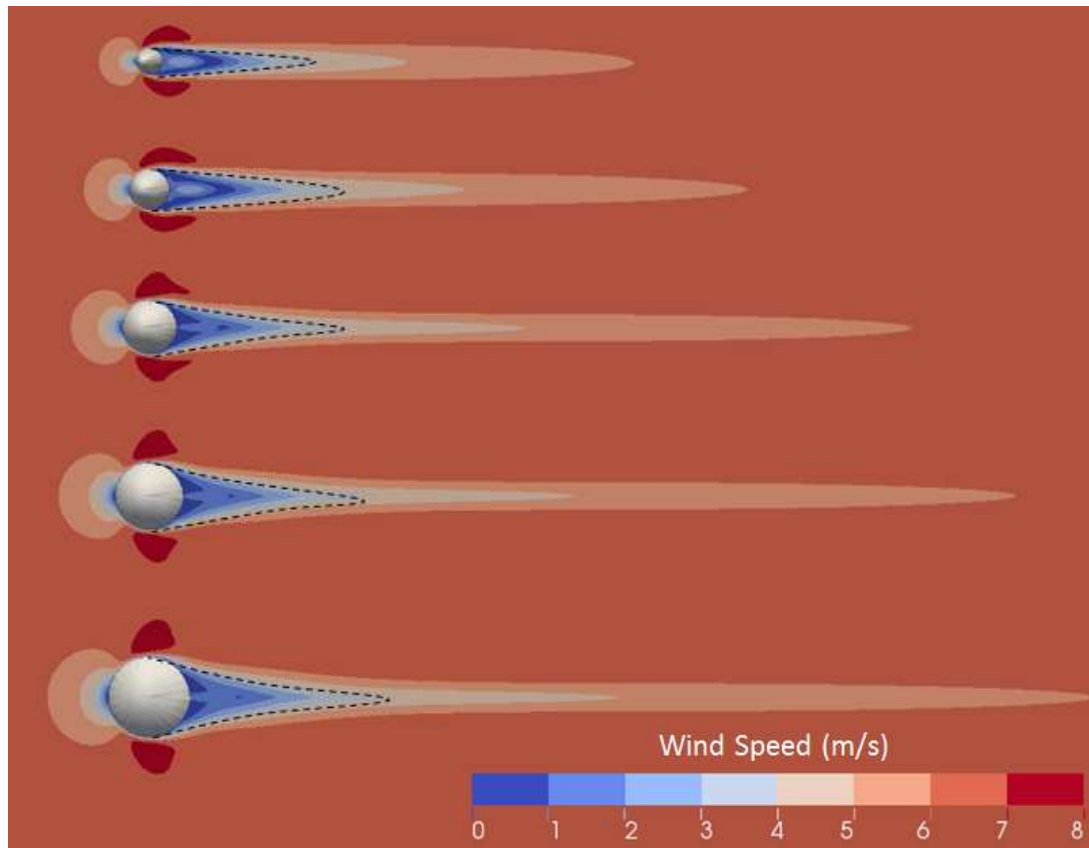


Figure 5. Zones of wind speed at 0.1 m above the surface for an incident wind speed of 10 m s^{-1} at 1 m above the surface. The dashed line depicts the extent of the wake zone within which a shadow dune forms. Nebkha diameter increases in 0.25 m increments from 0.5 m at the top to 1.50 m at the base. Shadow dune length and wake zone length increases gradually as nebkha diameter increases.

4.1 Horizontal flow structure

Fig. 5 illustrates a plan view of the wind speed zonnens at 0.1 m above the surface up- and downwind of the five nebkha for an incident wind of 10 m s^{-1} (at 1 m above the surface). The region within the dashed lines indicates the shadow zone defined as terminating downwind at a near surface wind speed of 4 m s^{-1} . The extent of the shadow zone as indicated by the dashed line, increases slightly with nebkha width, although there is little difference between the second and third nebkha. The length of the $4\text{-}5 \text{ m s}^{-1}$ zone displays a more regular increase in length with increasing nebkha width. Shadow dune length would therefore also increase as nebkha width increases. Note that as nebkha width increases, the zone of upwind flow deceleration expands, and the form of the high speed lateral (spanwise) or marginal flow

regions change from compressed elongate (delta-type) wings to wider arcuate (swept-type) wings. These differences in the flow structure probably reflect the differences in aspect ratio between the smaller and the larger width nebkhas, and also that the point of flow separation on the lateral margins moves upwind for the larger nebkha. The elongate high speed flow on the margins of the smallest nebkha cone compress the lateral (spanwise) extent of the downwind separation envelope creating a larger, longer, flame-like low velocity zone behind the nebkha compared to the other four larger nebkha.

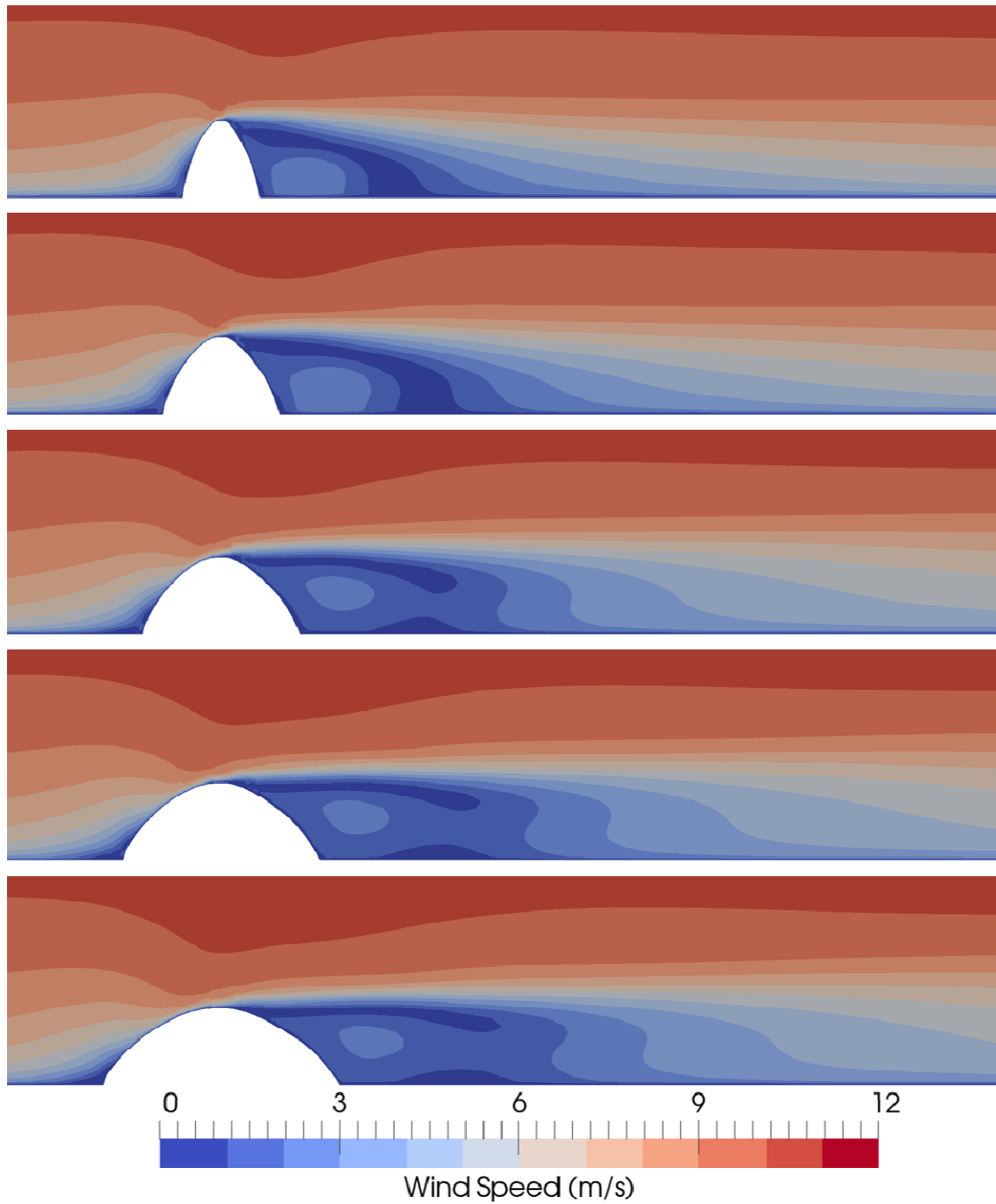


Figure 6. Vertical transect through centre axis of the computational domain for a wind speed of 10 m s^{-1} at 1 m above the surface at the inlet.

The morphologies of the nebkha are quite different to the more vertical cylinders studied by, for example, Sutton and Mckenna Neuman (2008) and Furieri et al. (2014), and thus the degree of turbulence in front of the nebkha is less than in their cases.

4.2 Vertical Flow Structure

Fig. 6 illustrates the flow patterns for the five nebkha in a vertical plane aligned along the central axis line. On average, the zone of low flow within the separation envelope downwind of the nebkha tends to scale to that of the horizontal flow shown in Fig. 5, and as found in other studies (e.g. Luo et al., 2012). In the case of the first two smallest nebkha (0.5 and 0.75m widths), the lowest velocity lee zone bounded by the 0 to 1 m s⁻¹ zone describes an arch extending from the leeward top of the nebkha down to the surface. Once the nebkha reaches 1.0 m wide and above, this lowest velocity lee zone comprises two separate parts; a narrow finger-like form extending downwind from the leeward top of the nebkha, and a small dome projecting above the surface some distance downwind of the nebkha. The lowest speed zone is also detached from the bed in the larger three nebkha compared to the two smaller nebkha.

4.3 Streamline Structure and Velocity Profiles

Fig. 7 shows the wind speed zones and streamlines at 0.1 m above the surface of the dune for an incident wind speed of 10 m s⁻¹ at 1 m above the surface. The location of the greatest vorticity in the paired symmetrical reversing flow vortices moves upwind with increasing nebkha width. Note that even in the case of the smallest nebkha, the leeward zone of lower than incident flow is extensive and it takes a considerable distance for full flow recovery to take place (Fig. 5). The central axis velocity profiles associated with two of the nebkha are displayed in Fig. 8 for comparison. The velocity profile structure is similar for the upwind positions at the nebkha toe and for the immediate downwind location where pronounced flow separation results in negative velocities and reversing flow. Flow recovery occurs more rapidly behind the smaller (0.75 m) nebkha compared to the larger 1.5 m-wide nebkha, and the profiles diverge in the lower near-bed region downwind (compare profiles at 2 m and 6 m). At around 15 m downwind, both velocity profiles are again similar (Fig. 8).

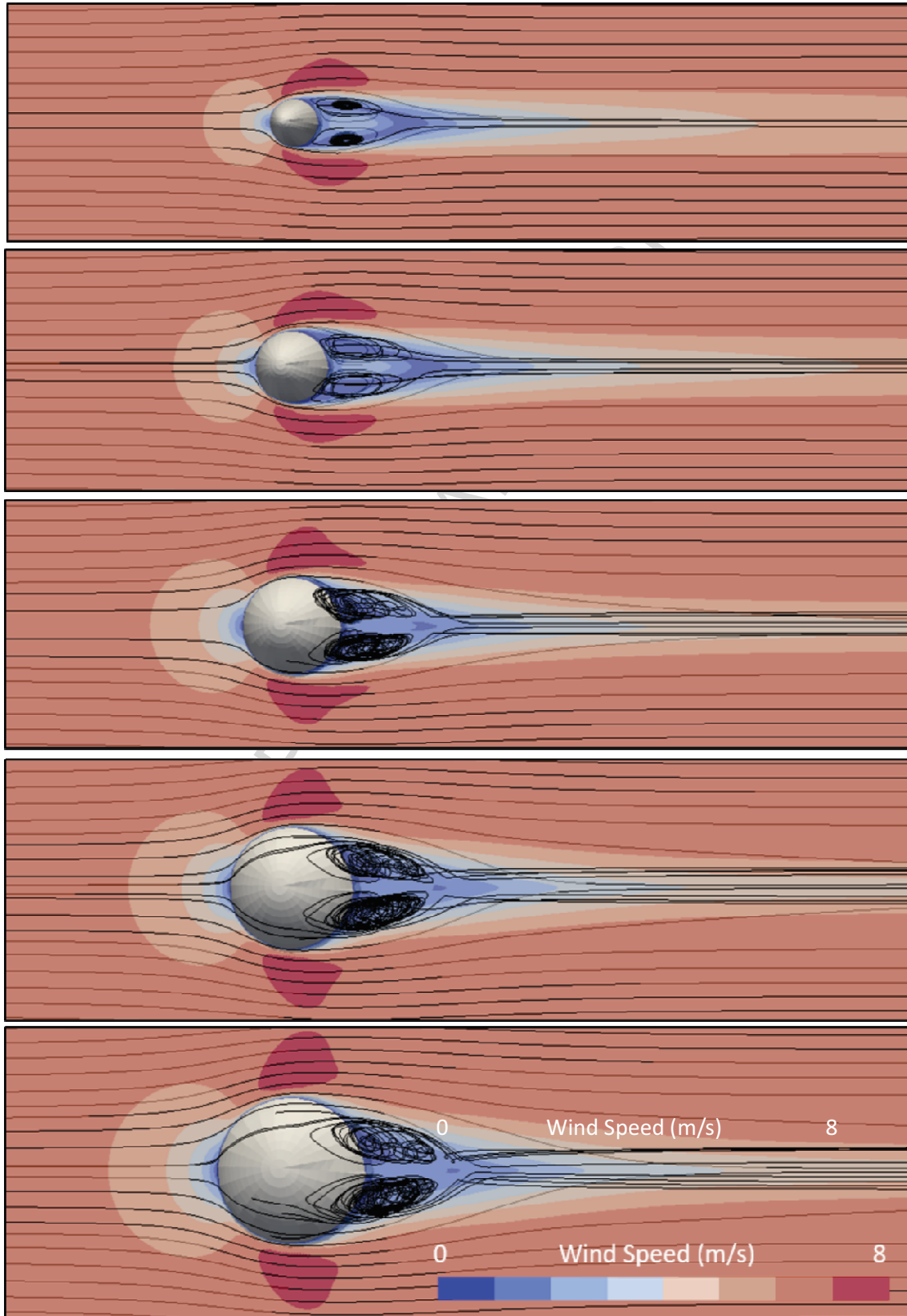


Figure 7. Wind speed at 0.1 m above the surface of the dune for a incident wind speed of 10 m s^{-1} at 1 m above the surface. Streamlines were seeded at 0.1 m above the surface upwind of the nebkha. Nebkha diameter increases in 0.25 m steps from 0.5 m at the top of the diagram to 1.50 m at the bottom. The location of the greatest vorticity in the paired symmetrical reversing flow vortices moves upwind with increasing nebkha width.

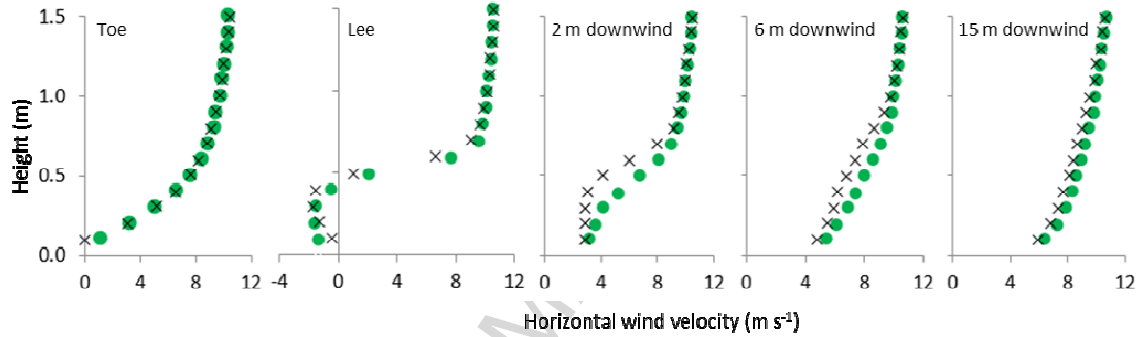


Figure 8. Wind velocity (u) profiles down the centreline axis for an incident wind speed of 10 m s^{-1} at 1 m above the surface at the inlet. Two examples are shown for the 0.75 m (dots) and 1.5 m (crosses) diameter nebkha.

4.4 Variations in Wind Velocity

Fig. 9 illustrates plots of wind velocity simulated at every 0.02 m upwind and downwind of the five nebkha for four incident wind velocities of 7.5, 10, 15 and 20 m s^{-1} . This was carried out to examine the effect of incident wind velocity on flow separation. The upwind incident wind begins to decrease first in the case of the largest nebkha and displays a consistent pattern with decreasing nebkha size or width. This is in line with the observed increasingly greater size of the upwind low velocity zone with increasing nebkha width as shown in Figs. 5 and 7. As incident wind velocity increases, the point where the chosen threshold velocity (4 m s^{-1}) occurs moves upwind and closer to the nebkha. In addition, as nebkha size decreases, the zone of flow separation decreases, and the threshold velocity point of 4 m s^{-1} obviously moves closer to the nebkha.

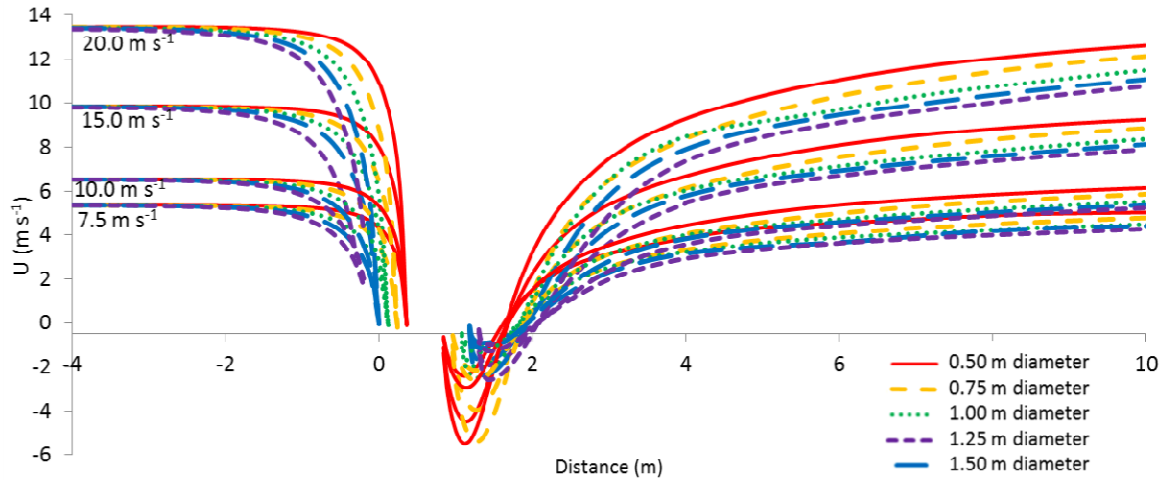


Figure 9. Wind velocity (u) at 0.1 m above the surface through the centreline of the computational domain for wind speeds of 7.5 m s^{-1} , 10 m s^{-1} , 15 m s^{-1} and 20 m s^{-1} at 1 m above the surface at the inlet. Each colour represents a different nebka diameter. Wind velocity was measured in the model at every 0.02 m from 4 m upwind to 10 m downwind.

4.5 Turbulent Kinetic Energy

Fig. 10 illustrates the variation in turbulent kinetic energy (TKE) measured just above the bed on the centreline at 0.02 m intervals downwind, starting from 4 m upwind, for the lowest and highest wind speeds modelled. Upwind and immediately adjacent to the nebka, there is a near-vertical increase in TKE for each incident wind velocity. This occurs in the upwind flow region (region (i) - see Introduction) where there is considerable flow stagnation and low pressure at and near the bed adjacent to the nebka. The upwind reaction distance to the large pressure change increases with increasing incident wind velocity. The TKE is also markedly greater for the higher incident wind velocity (20 m s^{-1} compared to 7.5 m s^{-1}). Notably the CFD model does not indicate flow reversal in front of the five nebka.

Immediately downwind of the nebka, in flow region (v) characterised by flow separation and reversing vortices, the TKE increases for each of the nebka diameters at an incident wind velocity of 7.5 m s^{-1} . The increase is not uniform and is relatively higher for the smaller of the two nebka (Fig. 10). At an incident flow velocity of 20 m s^{-1} the TKE is significantly greater behind the nebka compared to the 7.5 m s^{-1} flow. In addition, the TKE results are separated into two groups. The TKE is substantially greater for the two smaller nebka (0.5

and 0.75 m diameters) compared to the significantly lower TKE measured downwind of the medium to larger nebkha (1.0 to 1.5m diameter).

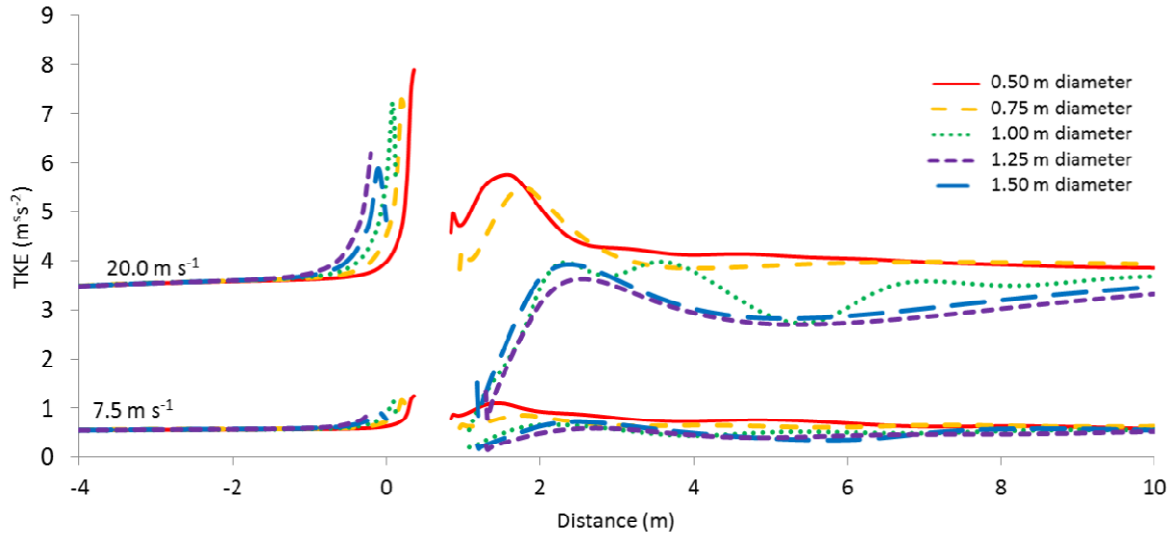


Figure 10. Turbulent kinetic energy (TKE) at 0.1 m above the surface through the centreline of the computational domain for wind speeds of 7.5 m s^{-1} and 20 m s^{-1} at 1 m above the surface at the inlet. Each colour represents a nebkha diameter. TKE was measured at every 0.02 m. The TKE is substantially different for the two smallest nebkha at the higher 20 m s^{-1} incident velocity.

The results shown in Figs. 9 and 10 when combined with those presented in Fig. 5 indicate that the position of the coherent, symmetrical flow reversal vortices produced behind the two smaller nebkha (0.5 m, 0.75 m) are influencing the structure of wake development. In Figs. 5 and 7, the core regions of the reversing vortices are situated further downwind behind the smaller nebkha (0.5 m, 0.75 m) than in the case of the larger nebkha (1.0 m, 1.25 m, 1.5 m). In addition, the lateral ‘wings’ of high velocity change shape from a streamwise (downwind) extension to a spanwise (acrosswind) extension. These factors in combination may allow for the higher velocity perturbations (TKE) behind the smaller nebkha, and the suppression of downwind wake development in the case of the increasingly larger nebkha. This results in the threshold value of 4 m s^{-1} being reached at a similar position behind the larger nebkha once incident wind velocities are above $\sim 10\text{--}12 \text{ m s}^{-1}$.

5.0 Relationships between Nebkha flow and Shadow Dune length

For this study, the termination point for the shadow dune (shadow dune length) is taken to be the point in the horizontal reversing wake region where the velocity reaches 4 m s^{-1} (following Hesp, 1981). Shadow dune length varies both as a function of nebkha width and wind velocity (Fig. 11).

Nebkha diameter or spanwise width affects shadow dune length up to at least an incident wind velocity of 10 m s^{-1} , and subsequently has little effect at higher wind speeds. At the lowest wind velocity of 7.5 m s^{-1} shadow dune length increases by 50% between a nebkha diameter of 0.5 m and 1.5 m. As wind velocity increases, the effect of nebkha diameter or width is rapidly reduced such that there is only a 25% increase in shadow dune length at 10 m s^{-1} , 15% at 15 m s^{-1} and 13.5% at 20 m s^{-1} between the 0.5 and 1.5 m-diameter nebkhas (Fig. 8). Hesp (1981) examined a significantly smaller range of plant widths than the nebkha modelled herein. His plant widths ranged from 7 to 19 cm diameter with aspect ratios (h/D) of 10, 5.8, 4.6 and 3.6, and showed that for an incident wind velocity of 7 m s^{-1} shadow dune length increased by ~29% between a 7 cm and a 19 cm plant width. This percentage increase in shadow dune length as a function of plant width was roughly maintained (typically ~25%) through the range of wind speeds up to 20 m s^{-1} measured by Hesp (1981; see his Fig. 6). However, Hesp's curves were approximately curvilinear or Z-shaped. Dong et al. (2008) found that their vertical reverse cells changed mainly as a function of shrub density and only slightly with wind velocity.

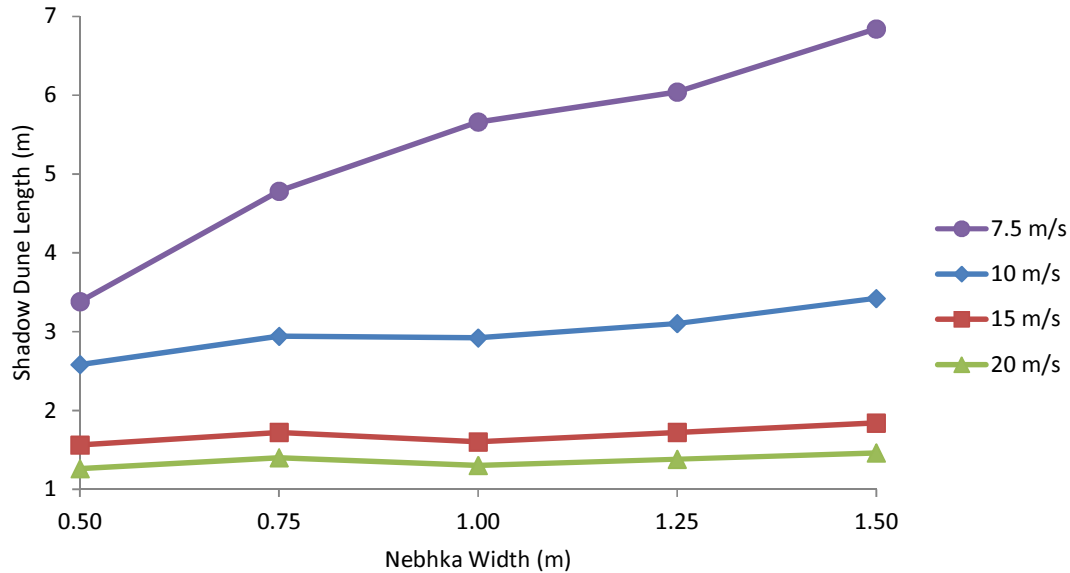


Figure 11. Estimation of shadow dune length in lee of the various nebkha assuming a threshold velocity of 4.0 m s^{-1} at 0.1 m above the surface where shadow dune construction would terminate. Shadow dune length increases as nebkha width increases for the 7.5 m s^{-1} incident flow, slightly for the 10 m s^{-1} flow, and is not affected by nebkha width at higher flows. Flow velocity affects shadow dune length most at lower velocities.

Shadow dune length more strongly varies as a function of wind velocity. For example, for a 1.0 m diameter nebkha (h/D of 0.5), shadow dune length is 1.3 m at 20 m s^{-1} , 1.6 m at 15 m s^{-1} , 2.9 m at 10 m s^{-1} , and 5.6 m at 7.5 m s^{-1} . As noted by Hesp (1981), the higher the incident wind speed, the shorter the shadow dune for any particular plant or nebkha diameter or width. In contrast, for the vertical case, Dong et al. (2008) examined wind tunnel flow through and around a single ‘plant’ formed of 1 mm rigid stalks 20 mm high of varying densities placed within a 50 mm diameter circular base and found that the structure of *vertical* reverse cells varied only slightly with wind velocity.

6.0 Discussion

The value of this approach in utilising CFD to examine the flow structure around nebkha lies in the ability it provides to examine a range of defined nebkha morphologies, rarely presented in the field in any systematic way, a range of wind velocities in a uni-directional incident flow regime, and the more detailed visualization of the flow fields and structure. While this

study has limitations due to the lack of vegetation on the nebkha, the conclusions in the Hesp (1981) study regarding the relationship between shadow dune length and wind velocity are largely supported in this present study. However, Hesp (1981) found that shadow dune length was determined more by nebkha or plant width rather than wind velocity (as found in this study) for a range of small nebkha up to 20cm diameter.

New findings on the nature of the flow structure for varying nebkha morphologies and incident wind velocities have been revealed. For example, the location of the greatest vorticity in the paired lee vortices moves upwind with increasing nebkha width, the shape of the marginal high velocity zones (the lateral ‘wings’) change shape from a streamwise (downwind) extension to a spanwise (acrosswind) extension with an increase in nebkha diameter, and the vertical flow structure in the shadow zone behind the nebkha also varies with nebkha diameter. These factors in combination may allow for the higher velocity perturbations (TKE) behind the smaller nebkha, and the suppression of downwind wake development in the case of the increasingly larger nebkha.

7.0 Conclusions

The following conclusions may be made:

1. While the CFD modelling conducted here cannot mimic the various levels of bleed flow that occur through plants of varying densities on the surface of a nebkha, nebkha shapes can be reasonably represented.
2. The mean flow is characterised by two symmetrically opposed vortices within a flow separation wake zone at the high Reynolds numbers investigated and modelled here;
3. The aspect or shape ratio of the nebkha influences the nature of the horizontal and vertical flow structure as also found by Luo et al. (2012). In the present study, the lowest velocity flow zone in the vertical plane behind the two smallest nebkha approximates an arch, whereas once the nebkha reaches 1.0 m wide and above, this lowest velocity lee zone displays two segments with the upper larger one characterised by a finger-like form, perhaps due to the change in aspect ratio;
4. The horizontal flow structure behind the smallest (0.5 m width) nebkha displays a flame-like pattern compared to the larger four nebkha which display a triangular

- shape. This result differs from that of Luo et al. (2012) who found that the horizontal reverse flow area was wider behind a thin obstacle than behind a thick obstacle;
5. Flow recovery occurs more rapidly behind the smaller nebkha compared to the larger nebkha;
 6. The location of the greatest vorticity in the lee wake region moves upwind with increasing nebkha width;
 7. Shadow dune length is most affected by nebkha width at low wind velocities. Length increases as nebkha width increases for a 7.5 m s^{-1} incident flow, slightly for a 10 m s^{-1} flow, and is barely affected by nebkha width at higher flows (cf. Hesp, 1981);
 8. As wind velocity increases, the effect of nebkha diameter or width is rapidly reduced such that there is only a 25% increase in shadow dune length at 10 m s^{-1} , 15% at 15 m s^{-1} and 13.5% at 20 m s^{-1} between the 0.5 and 1.5 m diameter nebkhas;
 9. Shadow dune length more strongly varies as a function of wind velocity rather than nebkha diameter. For example, for a 1.0 m diameter nebkha (h/D of 0.5), shadow dune length is 1.3 m long at 20 m s^{-1} , 1.6 m long at 15 m s^{-1} , 2.9 m long at 10 m s^{-1} , and 5.6m long at 7.5 m s^{-1} .
 10. Additional field and CFD research examining a range of nebkha morphologies with differing vegetation species and densities (and therefore a variety of bleed flow conditions) is required to further validate these findings.

Acknowledgements

Thanks to Flinders University for funding this project, and to OLU for his continued ministry. Thanks also to Cheryl Mckenna-Neuman, an anonymous reviewer, and Andrew Plater for their valued assistance and suggestions to improve the manuscript.

References

- Acarlar, M. S., Smith, C.R., 1987. A study of hairpin vortices in a laminar boundary layer. Part 1. Hairpin vortices generated by a hemisphere protuberance. *Journal of Fluid Mechanics*, 175, pp 1-41. doi:10.1017/S0022112087000272

- Al-Awadhi, J. M., Al-Dousari, A.M., 2013. Morphological characteristics and development of coastal nabkhas, north-east Kuwait. *International Journal of Earth Sciences* 102, (3), 949-958.
- ANSYS, 2013. ANSYS Fluent Theory Guide, 15.0 Edn., ANSYS Inc., 2013.
- Bagnold, R.A., 1954. *The Physics of Blown Sand* (2nd Edn.) Methuen, London, 265p
- Bauer, B.O., Walker, I.J., Baas, A.C.W., Jackson, D.W.T., Mckenna Neuman, C., Wiggs, G.F.S., Hesp, P.A., 2013. Critical Reflections on the Coherent Flow Structures Paradigm in Aeolian Geomorphology. In: Venditti, J.G., Best, J.L., Church, M., Hardy, R.J. (Eds.), *Coherent Flow Structures at the Earth's Surface*, Wiley-Blackwell.
- Bouma, T.J., van Duren, L.A., Temmerman, S., Claverie, T., Blanco-Garcia, A., Ysebaert, T., Herman, P.M.J., 2007. Spatial flow and sedimentation patterns within patches of epibenthic structures: Combining field, flume and modelling experiments. *Continental Shelf Research* 27, 1020–1045.
- Blocken, B., Stathopoulos, T., Carmeliet, J., 2007. CFD simulation of the atmospheric boundary layer: wall function problems. *Atmospheric Environment*, 41, 238-252.
- Catalano, P., Wang, M., Iaccarino, G., Moin, P., 2003. Numerical simulation of the flow around a circular cylinder at high Reynolds numbers. *Heat and Fluid Flow* 24, 463-469.
- Chang, W.Y., Constantinescu, G., Tsai, W.F., 2014. LES of flow past a submerged circular patch of vegetation. In: Schleiss et al. (Eds.) *River Flow 2014. Intl. Conf. on Fluvial Hydraulics*. Taylor and Francis Group, London: 419-427.
- Chawdhury, S., Morgenthal, G., 2016. Flow reproduction using Vortex Particle Methods for simulating wake buffeting response of bluff structures. *J. of Wind Engineering and Industrial Aerodynamics* 151, 122-136.
- Cooke, R., Warren, A., Goudie, A., 1993. *Desert Geomorphology*. UCL Press, 526pp.

- Cooper, W.S., 1967. Coastal Dunes of California. Geological Society of America, Memoir 104, 131 pp.
- de Lima, P.H.S., Janzen, J.G., Nepf, H.M., 2015. Flow patterns around two neighbouring patches of emergent vegetation and possible implications for deposition and vegetation growth. *Environmental Fluid Mechanics* 15, 881-898.
- Dong, Z., Wanyin, L., Guangqiang, Q., Ping, L., 2008. Wind tunnel simulations of the three-dimensional airflow patterns around shrubs. *Journal of Geophysical Research* 113: F202016, doi: 10.1029/2007JF000880
- El-Bana, M.I., Nijs, I., Kockelbergh, F., 2002. Microenvironmental and vegetational heterogeneity induced by phytogenic nebkhas in an arid coastal ecosystem. *Plant and Soil* 247, 283-293.
- Fu, C. L., Cheng, C. M., Lo, Y. L., Cheng, D. Q., 2015. LES simulation of hemispherical dome's aerodynamic characteristics in smooth and turbulence boundary layer flows. *Journal of Wind Engineering and Industrial Aerodynamics* 144, 53-61.
- Furieri, B., Harion, J.L., Milliez, M., Russeil, S., Santos, J.M., 2014. Numerical modelling of aeolian erosion over a surface with non-uniformly distributed roughness elements. *Earth Surfaces Processes and landforms* 39(2), 156-166. doi:10.1002/esp.3435
- Gillies, J. A., Lancaster, N., Nickling, W. G., Crawley, D. M., 2000. Field determination of drag forces and shear stress partitioning effects for a desert shrub (*Sarcobatus vermiculatus*, greasewood). *Journal of Geophysical Research: Atmospheres* 105, 24871-24880.
- Gillies, J. A., Nickling, W. G., King, J., 2002. Drag coefficient and plant form response to wind speed in three plant species: Burning Bush (*Euonymus alatus*), Colorado Blue Spruce (*Picea pungens glauca.*), and Fountain Grass (*Pennisetum setaceum*). *Journal of Geophysical Research: Atmospheres* 107. doi:10.1029/2001JD001259.

- Gillies, J. A., Nield, J. M., Nickling, W. G., 2014. Wind speed and sediment transport recovery in the lee of a vegetated and denuded nebkha within a nebkha dune field. *Aeolian Research* 12, 135-141.
- Greeley, R., Iversen, J.D., 1985. Wind as a geological process on Earth, Mars, Venus and Titan. Cambridge Univ. Press, 333pp.
- Hesp, P.A., 1981. The formation of shadow dunes. *Journal of Sedimentary Research* 51, 101-111. doi: 10.1306/212F7C1B-2B24-11D7-8648000102C1865D.
- Hesp, P.A., 2002. Foredunes and Blowouts: initiation, geomorphology and dynamics. *Geomorphology* 48, 245-268.
- Hesp, P.A., 2004. Coastal dunes in the Tropics and Temperate Regions: Location, formation, morphology and vegetation processes. In: Martinez, M., Psuty, N. (Eds.), *Coastal Dunes, Ecology and Conservation*. Ecological Studies v. 171. Springer-Verlag, Berlin: 29-49.
- Hesp, P.A., 2013. Conceptual models of the evolution of transgressive dunefield systems. *Geomorphology* 199: 138–149.
- Hesp, P.A. and Mclachlan, A., 2000. Morphology, dynamics, ecology and fauna of *Arctotheca populifolia* and *Gazania rigens* nabkha dunes. *Journal of Arid Environments* 44, 155-172.
- Hesp, P.A., Martinez, M.L., Miot da Silva, G., Rodríguez-Revelo, N., Gutierrez, E., Humanes, A., Laínez, D., Montaña, I., Palacios, V., Quesada, A., Storero, L., González Trilla, G., Trochine, C., 2011. Transgressive dunefield landforms and vegetation associations, Doña Juana, Veracruz, Mexico. *Earth Surface Processes and Landforms* 36, 3, 285–295.
- Hesp, P.A., Smyth, T.A.G., in press. Dunes created by vegetation and topography. In: Livingstone, I., Warren, A., (Eds.), *Aeolian Geomorphology: a New Introduction*.

- Hesp, P.A., Walker, I.J., 2013. Aeolian environments: Coastal dunes. In: Shroder, J. (Editor in Chief), Lancaster, N., Sherman, D.J., Baas, A.C.W. (Eds.), *Treatise on Geomorphology*, vol. 11, *Aeolian Geomorphology*. Academic Press, San Diego, CA, pp. 109-133.
- Hesp, P.A., Walker, I.J., Chapman, C., Davidson-Arnott, R., and Bauer, B.O., 2013. Aeolian dynamics over a foredune, Prince Edward Island, Canada. *Earth Surface Processes and Landforms* 38, 1, 1566–1575.
- Hsu, S.A., 1973. Computing aeolian sand transport from shear velocity measurements. *J. Geology* 81, 739-743.
- Iversen, J.D., Wang, W.P., Rasmussen, K.R., Mikkelsen, H.E., Hasiuk, J.F., Leach, R.N., 1990. The effect of a roughness element on local saltation transport. *Journal of Wind Engineering and Aerodynamics* 36, 845–854.
- Jackson, D.W.T., Beyers, J.H.M., Lynch, K., Cooper, J.A.G., Baas, A.C.W., Delgado-Fernandez, I., 2011. Investigation of three-dimensional wind flow behaviour over coastal dune morphology under offshore winds using computational fluid dynamics (CFD) and ultrasonic anemometry. *Earth Surf. Process. Landforms* 36, 1113–1124. doi:10.1002/esp.2139
- Kharoua, N., Khezzar, L., 2013. Large Eddy Simulation Study of Turbulent Flow Around Smooth and Rough Domes. *Proc. IMeshE, Part C. Journal of Mechanical Engineering Science* 227, 2686-2700.
- Kiya, M., Sasaki, K., 1983. Structure of a turbulent separation bubble. *Journal of Fluid Mechanics*, 137, 83-113. doi:10.1017/S002211208300230X
- Leenders, J.K., Sterk, G., Van Boxel, J.H., 2011. Modelling wind-blown sediment transport around vegetation elements. *Earth Surface Processes and Landforms* 36, 1218-1229.

- Li, Z.S, Wu, S., Dale, J., Ge, L., He, M., Wang, X., Jin, J., Liu, J., Li, W., Ma, R., 2008a.
Wind tunnel experiments of air flow patterns over nabkhas modeled after those from the Hotan river basin, Xinjiang, China (I): non-vegetated. *Front Earth Sci. China* 2, 333–339.
- Li, Z.S., Wu, S., Dale, J., Ge, L., He, M., Wang, X., Jin, J., Liu, J., Li, W., Ma, R., 2008b.
Wind tunnel experiments of air flow patterns over nabkhas modeled after those from the Hotan river basin, Xinjiang, China (II): vegetated. *Front Earth Sci. China* 2, 340–345.
- Luo Wanyin, Dong Zhibao, Qian Guangqiang and Lu Junfeng., 2012. Wind tunnel simulation of the three-dimensional airflow patterns behind cuboid obstacles at different angles of wind incidence, and their significance for the formation of sand shadows. *Geomorphology* 139-140, 258-270. doi:10.1016/j.geomorph.2011.10.027.
- Luo WanYin, Dong ZhiBao, Qian GuangQiang, Lu, Junfeng., 2014. Near-wake flow patterns in the lee of adjacent obstacles and their implications for the formation of sand drifts: a wind tunnel simulation of the effects of gap spacing. *Geomorphology* 213, 190–200. doi:10.1016/j.geomorph.2014.01.008.
- McKenna Neuman, C., Bédard, O., 2015. A wind tunnel study of flow structure adjustment on deformable sand beds containing a surface-mounted obstacle. *Journal of Geophysical Research: Earth Surface* 120, (9), 1824-1840.
- Maun, M.A., 2009. *The Biology of Coastal Sand Dunes*. Oxford Univ Press, 265pp.
- Mayaud, J.R., Wiggs, G.F.S., bailey, R.M., 2016. Characterizing turbulent wind flow around dryland vegetation. *Earth Surface Processes and Landforms* 41, 1421-1436.
- Melton, F.A., 1940. A tentative classification of sand dunes: its application to dune history in the Southern High Plains. *J. Geology* 48, 113-174.
- Meneghini, J. R., Saltara, F., Siqueira, C. L. R., Ferrari, J. A., 2001. Numerical simulation of flow interference between two circular cylinders in tandem and side-by-side arrangements. *Journal of fluids and structures* 15 (2), 327-350.

- Mountney, N. P., Russell, A. J., 2009. Aeolian dune-field development in a water table-controlled system: Skeiðarársandur, Southern Iceland. *Sedimentology* 56 (7), 2107-2131.
- Nepf, H.M., 2012. Flow and Transport in Regions with Aquatic Vegetation. *Annual Review of Fluid Mechanics* 44, 123 -142.
- Nichols, R.L., 1969. Geomorphology of Inglefield land, North Greenland. *Meddelelser om Grønland* 188 (1), 1-109.
- Nickling, W. G., Wolfe, S. A., 1994. The morphology and origin of nabkhas, Region of Mopti, Mali, West Africa. *J. Arid Environments* 28, 13–30.
- Nield, J.M., Baas, A.C.W., 2008. Investigating parabolic and nebkha dune formation using a cellular automaton modelling approach. *Earth Surface Processes and Landforms* 33, 724-740.
- Niemann, H-J, Holscher, N., 1990. A review of recent experiments on the flow past circular cylinders. *Journal of Wind Engineering and Industrial Aerodynamics* 33, 1-2, 197-209
- Okamoto, T., Fujimoto, Y., Toda, K., Nezu, I., 2014. Development of coherent structure and turbulence behind a finite-length emergent vegetation patch in open-channel flow. In: Schleiss et al. (Eds.) *River Flow 2014. Intl. Conf. on Fluvial Hydraulics*. Taylor and Francis Group, London: 437-443.
- Ortiz, A., Ashton, A., Nepf, H., 2013. Mean and Turbulent Velocity Fields Near Rigid and Flexible Plants, and the Implications for Deposition. *J. Geophys. Research. Earth Surface*, 118, 1-15:
- Palau-Salvador, G., Stoesser, T., Frohlich, J., Kappler, M., Rodi, W., 2009. Large eddy simulations and experiments of flow around finite-height cylinders. *Flow, Turbulence and Combustion*, 84(2), 239-275.

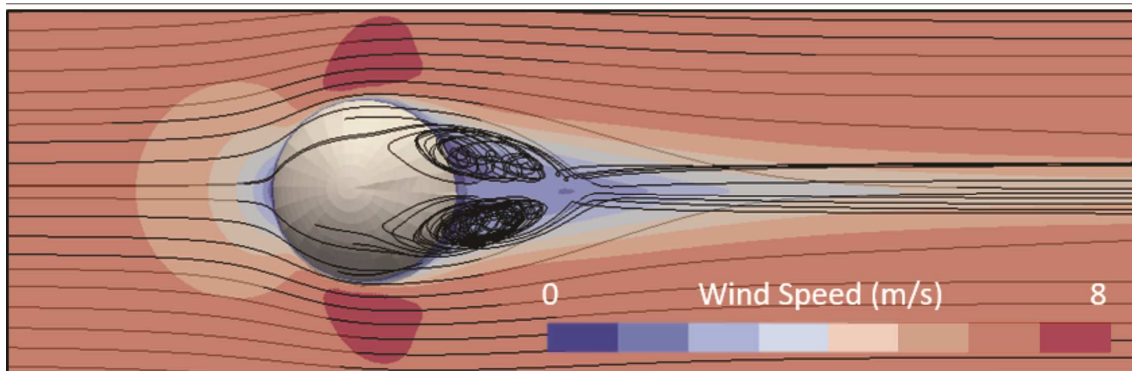
- Patankar, S.V., Spalding D.B., 1972. A calculation procedure for heat, mass and momentum transfer in three-dimensional parabolic flows. *International Journal of Heat and Mass Transfer* 15, 10, 1787-1806.
- Pidgeon, I.M., 1940. The ecology of the central coastal area of NSW III. Types of primary succession. *Proceedings Linnean Soc. NSW LXV*, 221-249.
- Poggi, D., Porporato, A., Ridolfi, L., Albertson, J.D., Katul, G.G., 2004. The effect of vegetation density on canopy sub-layer turbulence. *Boundary- Layer Meteorology* 111, 565–587.
- Poggi, D., Krug, C., & Katul, G. G., 2009. Hydraulic resistance of submerged rigid vegetation derived from first-order closure models. *Water Resources Research* 45 (10).
- Rango, A., Chopping, M., Ritchie, J., Havstad, K., Kustas, W., Schmugge, T., 2000. Morphological characteristics of shrub coppice dunes in desert grasslands of southern New Mexico derived from scanning LIDAR. *Remote Sensing of Environment* 74 (1), 26-44.
- Ranwell, D.S., 1972. *Ecology of salt marshes and sand dunes*. Chapman and Hall, London, 258pp.
- Richards, P.J., Hoxey, R.P., 1993. Appropriate boundary conditions for computational wind engineering models using the k- turbulence model. *Journal of Wind Engineering and Industrial Aerodynamics* 46, 145-153. doi:[http://dx.doi.org/10.1016/0167-6105\(93\)90124-7](http://dx.doi.org/10.1016/0167-6105(93)90124-7)
- Rodi, W., 1997. Comparison of LES and RANS calculations of the flow around bluff bodies. *Journal of Wind Engineering and Industrial Aerodynamics* 69-71, 55-75
- Rubin, D.M., Hesp, P.A., 2009. Multiple origins of linear dunes and implications for dunes on Titan. *Nature Geoscience* 2 (9), 653-658. doi:10.1038/ngeo610
- Ruz, M-H, Hesp, P.A., 2014. Geomorphology of high latitude coastal dunes, In: Martini, I.P., Wanless, H.R. (Eds.) *Sedimentary Coastal Zones from High to Low Latitudes:*

- Similarities and Differences. The Geological Society London, Spec. Publications 388, doi:10.1144/SP388.17
- Salisbury, E., 1952. *Downs and Dunes. Their Plant Life and Environment*. G. Bell and Sons, London.
- Savory, E., Toy, N., 1986. The flow regime in the turbulent wake of a hemisphere. *Experimental Fluids* 4, 181-188.
- Smyth, T.A.G, 2016, A review of Computational Fluid Dynamics (CFD) airflow modelling over aeolian landforms. *Aeolian Research* 22, 153-164. <http://dx.doi.org/10.1016/j.aeolia.2016.07.003>
- Smyth, T.A.G., Jackson, D.W.T., Cooper, J.A.G., 2013. Three dimensional airflow patterns within a coastal trough-bowl blowout during fresh breeze to hurricane force winds. *Aeolian Res.* 9, 111–123. doi:10.1016/j.aeolia.2013.03.002
- Sokolov, N.A., 1884. *Dunes – Formation, Development and Internal Structure*. Trudy Geologicheskogo Komiteta 9/2. St. Petersburg.
- Stringer, R. M., Zang, J., Hillis, A. J., 2014. Unsteady RANS computations of flow around a circular cylinder for a wide range of Reynolds numbers. *Ocean Engineering*, 87, 1-9.
- Sumner, D., Heseltine, J.L., Dansereau, O.J.P., 2004. Wake structure of a finite circular cylinder of small aspect ratio. *Exp. Fluids* 37 (5), 720-730.
- Sutton, S.L.F., McKenna Neuman, C. 2008. Sediment entrainment to the lee of roughness elements: Effects of vortical structures. *Journal of Geophysical Research* 113, F02S09, doi:10.1029/2007JF000783.
- Tavakol, M.M., Yaghoubi, M., Masoudi Motlagh, M., 2010. Air flow aerodynamic on a wall-mounted hemisphere for various turbulent boundary layers. *Exp. Thermal and Fluid Science* 34, 538-553.

- Tavakol, M., Abouali, M. O., Yaghoubi, M., 2015. Large eddy simulation of turbulent flow around a wall mounted hemisphere. *Applied Mathematical Modelling* 39 (13), 3596-3618.
- Thomas, P., Veverka, J., Lee, S., Bloom, A., 1981. Classification of wind streaks on Mars. *Icarus* 45(1), 124-153.
- Tsoar H. Critical Environments: Sand Dunes and Climate Change., 2013 In: John F. Shroder (Editor-in-chief), Lancaster, N., Sherman, D.J., and Baas, A.C.W. (Volume Editors). *Treatise on Geomorphology, Vol 11, Aeolian Geomorphology*, San Diego: Academic Press; 2013. p. 414-427.
- Vogel, S., 1994. *Life in Moving Fluids (2nd Edn.)*. Princeton University Press, 467pp.
- Warren, A., 1988. A note on vegetation and sand movement in the Wahiba sands. *Journal of Oman Studies, Special Rept 3*, 251-255.
- Wang, X. Wang, T. Dong, Z., Liu, X., Qian, G., 2006. Nebkha development and its significance to wind erosion and land degradation in semi-arid northern China. *J. Arid Environments* 65, 129–141.
- Weller, H.G., Tabor, G., Jasak, H., Fureby, C., 1998. A tensorial approach to computational continuum mechanics using object-oriented techniques. *Computers in Physics* 12, 620–631.
- Williamson, C.H.K., 1996. Vortex dynamics in the cylinder wake. *Annual Review Fluid Mechanics* 28, 477-539.
- Wolfe, S. A., Nickling, W. G., 1996. Shear stress partitioning in sparsely vegetated desert canopies. *Earth Surface Processes and Landforms* 21(7), 607-619.

- Wyatt, V. E., Nickling, W. G., 1997. Drag and shear stress partitioning in sparse desert creosote communities. *Canadian Journal of Earth Sciences* 34(11), 1486-1498.
- Xiao, J., Qu, J.J., Yao, Z.Y., Pang, Y., Zhang, K., 2015. Morphology and formation mechanism of sand shadow dunes on the Qinghai-Tibet Plateau. *J. Arid Land* 7 (1), 10-26.
- Xu, C-Y, Chen, L-W., Lu, X-Y., 2007. Large-eddy and detached-eddy simulations of the separated flow around a circular cylinder. *J. of Hydrodynamics Ser.B*, 19(5), 559-563.
- Yager, E.M., Schmeckle, M.W., 2013. The influence of vegetation on turbulence and bed load transport. *J. geophysical research: earth Surface* 118, 1585-1601.
- Zdravkovich, M.M., 1990. Conceptual overview of laminar and turbulent flows past smooth and rough circular-cylinders. *J. Wind Eng. Ind. Aerodynamics* 33, 53-62.
- Zou, X., Li, J., Liu, B., Zhang, C., Cheng, H., Wu, X., Kang, L., Wang, R., 2016. The protective effects of nebkhas on an oasis. *Aeolian Research* 20, 71-79.

Graphical abstract



ACCEPTED MANUSCRIPT

Highlights

Wind flow is modelled via CFD over five 'nebkha' dune forms

The flow structure within the leeward flow separation region is examined to better understand shadow dune formation.

Shadow dune length increases for low velocity incident flow but is affected little by higher velocity flow.

The location of the greatest vorticity in the paired lee vortices moves upwind with increasing nebkha width.

The shape of the marginal high velocity zones (the lateral 'wings') changes with an increase in nebkha diameter.

ACCEPTED MANUSCRIPT